# Computational study of pH-dependent oligomerization and ligand binding in Alt a 1, a highly allergenic protein with a unique fold

**María Garrido-Arandia · Jorge Bretones · Cristina Gómez-Casado**
**Nuria Cubells · Araceli Díaz-Perales · Luis F. Pacios**

**Abstract** Alt a 1 is a highly allergenic protein from *Alternaria* fungi responsible for several respiratory diseases. Its crystal structure revealed a unique β-barrel fold that defines a new family exclusive to fungi and forms a symmetrical dimer in a butterfly-like shape as well as tetramers. Its biological function is as yet unknown but its localization in cell wall of *Alternaria* spores and its interactions in the onset of allergy reactions point to a function to transport ligands. However, at odds with binding features in β-barrel proteins, monomeric Alt a 1 seems unable to harbor ligands because the barrel is too narrow. Tetrameric Alt a 1 is able to bind the flavonoid quercetin, yet the stability of the aggregate and the own ligand binding are pH-dependent. At pH 6.5, which Alt a 1 would meet when secreted by spores in bronchial epithelium, tetramer-quercetin complex is stable. At pH 5.5, which Alt a 1 would meet in apoplast when infecting plants, the complex breaks down. By means of a combined computational study that includes docking calculations, empirical p*K*a estimates, Poisson–Boltzmann electrostatic potentials, and Molecular Dynamics simulations, we identified a putative binding site at the dimeric interface between subunits in tetramer. We propose an explanation on the pH-dependence of both oligomerization states and protein–ligand affinity of Alt a 1 in terms of electrostatic variations associated to distinct protonation states at different pHs. The uniqueness of this singular protein can thus be tracked in the combination of all these features.

**Keywords** Allergenic proteins · Oligomerization · Protein–ligand binding · Electrostatic potentials · Molecular dynamics · Ligand–protein docking

**Abbreviations**

| | |
|---|---|
| 3D | Three-dimensional |
| APBS | Adaptive Poisson–Boltzmann solver |
| DPBA | Diphenylboric acid 2-aminoethyl ester |
| MD | Molecular dynamics |
| PB | Poisson–Boltzmann |
| PDB | Protein data bank |
| PISA | Proteins, interfaces, structures, and assemblies |
| PTGL | Protein topology graph library |
| RMSD | Root mean square deviation |
| RMSF | Root mean square fluctuation |

## Introduction

*Alternaria* is a genus of common molds that invade crops at pre- and post-harvest stages causing considerable agricultural spoilage due to rotting of fruits and vegetables. *Alternaria* sp. are also associated with respiratory allergies and severe asthma. Their spores can reach levels of

thousands per cubic meter of air during spring and summer months becoming a risk factor for respiratory diseases [1–7]. *A. alternata* is the most important member and one of the principal fungal agents associated with allergic disease. In the U.S., its presence is one of the most common causes of respiratory disorders, particularly in children and young adults [4–6]. In Southern Europe, over 20 % of patients with a history of respiratory allergy are sensitized to *A. alternata* [7].

Alt a 1 is the major allergen of *A. alternata* [8–11]. It is a highly allergenic protein that leads to IgE-mediated hypersensitivity in more than 90 % of patients with *Alternaria* sp. allergy [12]. Alt a 1 was cloned and the expressed recombinant allergen used to measure IgE and IgG antibody responses in *Alternaria*-sensitized patients [8–10]. Four linear epitopes were identified by synthetic overlapping peptides spanning the whole sequence of Alt a 1 and IgE binding was evaluated with sera from patients with *Alternaria*-induced allergy [13]. Two of these epitopes displayed consistent reactivity whereas two other regions showed weak IgE binding [13].

The high-resolution crystal structure of Alt a 1 reveals a unique 11-stranded β-barrel architecture that forms a "butterfly-like" homodimer [14]. Four cysteines form intramolecular disulfide bonds that contribute to the high temperature stability of the protein while an N-terminal cysteine (C30) is able to form an intermolecular disulfide bond that links the two subunits in the dimer [14]. While not a prerequisite for allergenicity, dimerization might enhance the allergenic potential of a protein, as only one type of IgE should be required for cross-linking [15]. As shown below, the spatial location of the main epitopes in the dimeric structure is consistent with a putative cross-link interaction with IgE. The secondary structure elements identified through the recently reported NMR backbone $^{1}H$, $^{15}N$, and $^{13}C$ chemical shift assignment of Alt a 1 in solution are in close agreement with the crystal structure [16]. Because searches with several structural alignment methods predicted rather low similarities, it has been claimed that the Alt a 1 structure is unique and defines a new protein family exclusively found in fungi [14]. As the structural study presented in the current work suggests, that uniqueness could also be tracked in the combination of oligomerization, intermolecular ligand-binding, and pH dependence features of this singular protein.

The biological function of Alt a 1 is still unknown. A search for 3D fragments did not show any functional relationship to enzymatic sites, ligand-binding sites, or DNA-binding templates [14]. Alt a 1 is localized in the cell wall of *Alternaria* sp. spores [17] which access the respiratory tract to mediate allergic reactions. This localization is consistent with a previous suggestion that Alt a 1 would be involved in spore germination [18]. Considering the binding properties known for other β-barrel proteins, a function as a transporter of small ligands could be hypothesized. However, the β-barrel in Alt a 1 seems too narrow to harbor ligands. Although it was speculated that in solution the protein could feature an internal cavity [14], recent Molecular Dynamics (MD) calculations showed that the dimensions of the β-barrel remain small and fluctuate very little along simulation time [19]. The possibility that higher-order oligomeric assemblies such as tetramers could increase the flexibility of Alt a 1, which in turn should be related with its ligand-binding features was also tentatively suggested without further elaboration [14]. Indeed, we propose here that this seems to be the case.

On the basis of our experimental results showing that Alt a 1 protein binds the flavonoid quercetin and that its aggregation state is pH-dependent, we present here a computational study of Alt a 1 intended to elucidate its possible binding mode. We achieved this by means of docking calculations, computation of Poisson-Boltzmann electrostatic potentials, empirical p*K*a predictions, and MD simulations for distinct protein assemblies. By taking in consideration protein-quercetin complexes at different pH values, we suggest a possible binding mode of Alt a 1 and provide detailed insight into the pH dependence of both oligomerization states and ligand-binding abilities. Based upon all these results, we finally propose a picture on the possible protein stages which could be relevant to investigate physiological interactions of Alt a 1 involved in the onset of allergic reactions.

## Methods

### Structural analyses

The initial 3D structure of Alt a 1 was the crystal structure at 1.9 Å resolution PDB id. 3V0R [14]. Secondary structure was identified with DSSP [20, 21]. The topology diagram of Alt a 1 (Fig. 1) was prepared from that initially provided for the 3V0R entry by PDBSum [22, 23] web (www.ebi.ac.uk/pdbsum/). Searches for related topologies were conducted using the Protein Topology Graph Library (PTGL) [24] web (ptgl.uni-frankfurt.de/). Aggregation states of Alt a 1 were obtained with the Proteins, Interfaces, Structures and Assemblies (PISA) method [25, 26] implemented in PDBePISA server (www.ebi.ac.uk/msd-srv/prot_int/pistart.html). All molecular graphics were prepared and rendered with PyMOL 1.7.6 [27].

### Docking calculations

Initial geometry of quercetin was prepared with structural modeling tools in the UCSF Chimera 1.10.2 package [28]

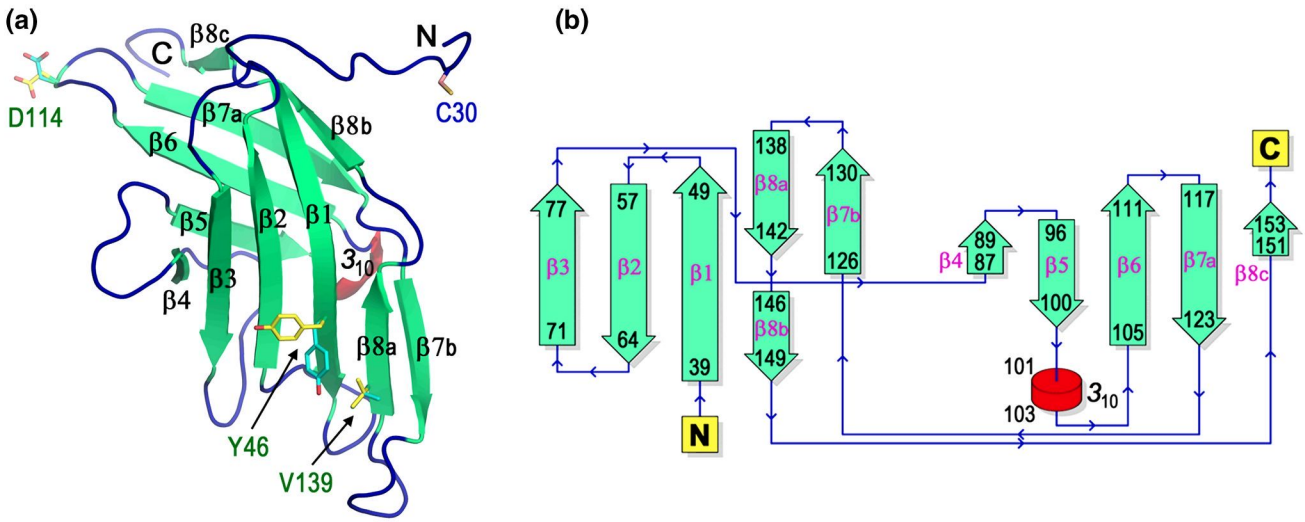


**Fig. 1** **a** Cartoon diagram of the crystal structure of Alt a 1 protein (PBD id 3V0R, [14]). Secondary structure assigned with DSSP. Labeling of β strands follow the notation used in Ref. [14]. Alternative conformations of side chains for Y46, D114, and V139 residues having 0.50 occupancy in the electron density are shown as sticks in yellow (conformation A) and cyan (conformation B). N-terminal C30 involved in dimer stabilization is also shown as sticks. **b** Topology diagram labelled as in **a** obtained from that given by PDBsum (www.ebi.ac.uk/pdbsum/)

while that of alternariol was taken from its crystallographic X-ray structure [29]. Both geometries were optimized in Molecular Mechanics calculations using AMBER ff14SB force field [30] after assigning AM1-BCC atomic charges with AnteChamber [31] as implemented in Chimera 1.10.2. Structures of quercetin and alternariol as well as the different protein aggregates were prepared for docking with AutoDockTools [32]. In order to explore putative binding sites, search spaces of sizes intended to enclose the whole structures were used in a first set of AutoDock Vina [33] docking calculations in monomeric and tetrameric Alt a 1. The monomer was explored by using a search space defined by a 50 Å edge cube centered at the center of the β-barrel whereas the tetramer was explored with an 80 Å edge cube centered at the center of the assembly. In both cases, the best docking poses (i.e., those having lowest protein–ligand binding affinities) for quercetin agreed well with the spatial positions of the crystallographic aromatic ligand (Fig. 2c) in both the X-ray structure of monomeric Alt a 1 [14] and in the PISA symmetry-predicted structure of tetrameric Alt a 1. With this result, a second set of AutoDock Vina [33] calculations were performed with smaller search spaces defined now by 20 Å edge cubes centered at the position of C6 atom of the crystallographic aromatic ligand in both monomeric and tetrameric Alt a 1. This procedure was used to obtain the geometries of quercetin and alternariol docked to tetrameric Alt a 1 with different protonation states corresponding to pH 5.5, 6.0, 6.5, and 7.0 (see below). In all cases, the docking pose with lowest protein–ligand binding affinity was selected for further analyses.

### Calculations of p*K*a values and protonation states

p*K*a values of ionizable side chain groups in Alt a 1 were computed with Propka 3.1 [34, 35] program. This version of the empirical p*K*a predictor Prop*K*a implements a new algorithm for modeling noncovalently coupled residues that due to their spatial proximity can influence the titration of each other [35]. A first run of Propka 3.1 for the three aggregation states of Alt a 1 predicted p*K*a values for all ionizable side chains and identified coupled residues while a second run of Propka 3.1 gave alternative p*K*a values for them. Propka 3.1 output also provides a list of interactions with other residues that result in each p*K*a particular value.

Protonation states at pH values given in input were assigned with Pdb2pqr 2.0.0 [36, 37] using Propka 3.1 as implemented in the Pdb2pqr server (nbcr-222.ucsd.edu/pdb2pqr_2.0.0/). Pdb2pqr adds hydrogens as needed by the particular protonation state and optimizes local conformations to fix clashes. Pdb2pqr/Propka 3.1 output takes the form of a PQR file that is just a modified PDB file in which occupancy and B-factor items in ATOM entries are replaced with atomic charges and radii. This PQR file is then used as input to compute Poisson-Boltzmann electrostatic potentials. For compatibility with the force field used in Molecular Dynamics simulations (see below), CHARMM 3.1 atomic charges [38] were selected in

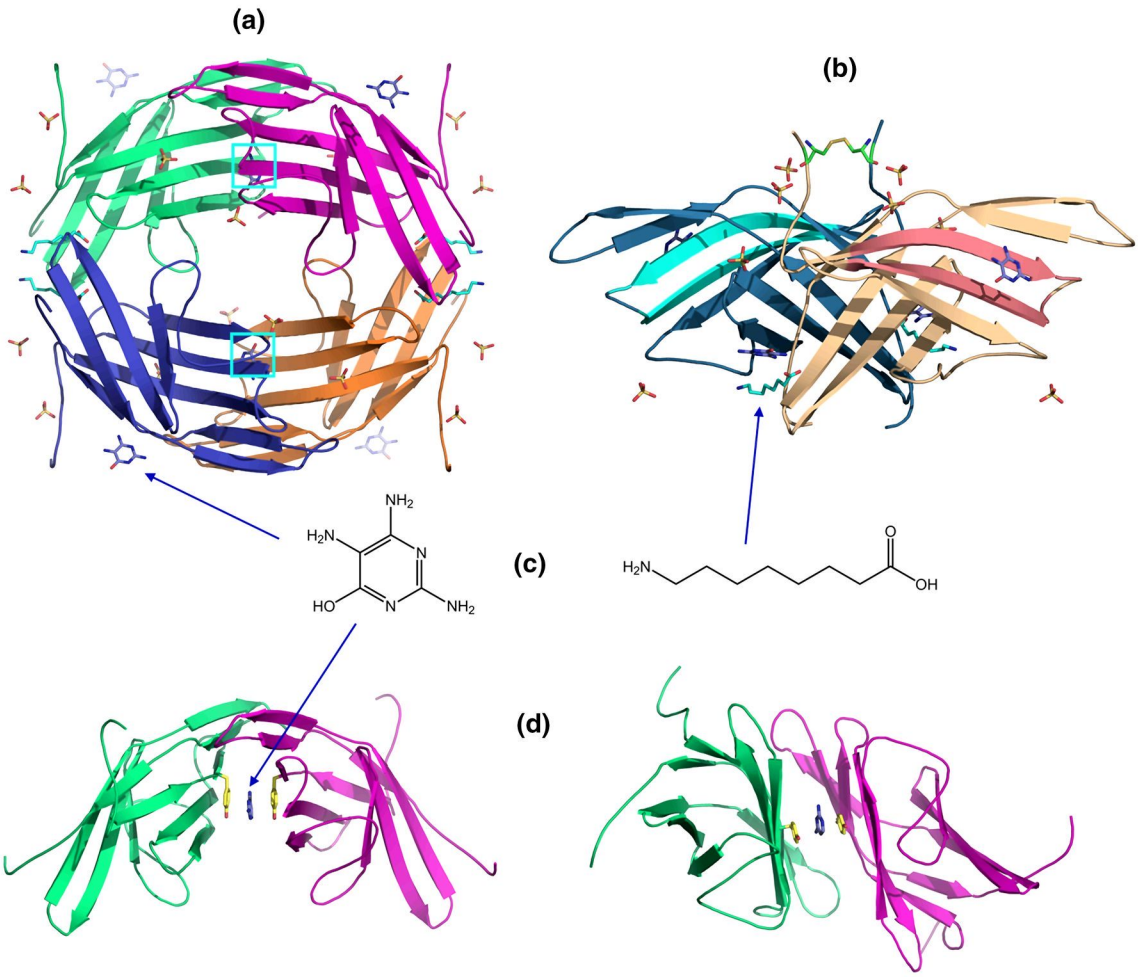


**Fig. 2** **a** Alt a 1 tetramer. Compounds originated from the crystallization solution depicted as sticks (sulfate anions in *yellow* and *red*) at spatial locations arisen from symmetry operations used to set oligomerization states. *Cyan boxes* mark the inter-subunit geometry of two molecules of one of these compounds. **b** Alt a 1 butterfly-like dimer. β-strands *colored* in different hues correspond to the two main epitope regions K41-P50 and Y54-K63 identified in the allergen [13]. The inter-monomer disulfide bridge formed between C30 residues in the two chains is represented as green sticks. **c** Structural formulas of compounds present in the crystal structure of Alt a 1: 4-hydroxy-2,5,6-triaminopyrimidine (*left*) and 8-aminocaprylic acid (*right*). **d** Upper (*left*) and side (*right*) views of the site marked in the *top cyan box* in **a** rotated to highlight the β-barrel substructure. Side chains of Y46 in their conformation B are represented as *yellow* (carbon bonds) and *red* (oxygens) sticks in the two subunit chains

Pdb2pqr calculations. Atom coordinates and charges for the different aggregates of Alt a 1 with protonation states corresponding to pH values from 4.0 to 7.0 at intervals of 0.5 pH units were obtained in this way. These tetramer structures corresponding to pH 5.5, 6.0, 6.5, and 7.0 were those used in docking calculations to obtain complexes with quercetin and alternariol as explained above.

### Poisson-Boltzmann electrostatic potentials

PB electrostatic potentials were computed for tetrameric Alt a 1-quercetin complexes at pH 5.5, 6.0, 6.5, and 7.0 by solving the Poisson–Boltzmann equation with APBS (Adaptive Poisson Boltzmann Solver) 1.4.1 program [39]. CHARMM 3.1 charges and radii [38] were assigned to protein atoms with Pdb2pqr/Propka 3.1 as explained above. CHARMM 3.1 force field parameters including atomic charges were assigned to quercetin and alternariol with the SwissParam method [40] implemented as a separate web service in Swiss Institute of Bioinformatics (swissparam.ch/). Radii for atoms in quercetin and alternariol were taken from values for equivalent atom types in PQR files for proteins. The nonlinear PB equation was solved in sequential focusing multigrid calculations in 3D meshes of $192^3 = 7{,}077{,}888$ points (spatial grids with step size about 0.5 Å in tetramer systems) at 298.15 K and 0.150 M ionic concentration. Dielectric constants 4 for proteins and 78.54 for water were used. The numerical output of all PB

electrostatic potentials were stored in OpenDX scalar data format and then mapped onto molecular surfaces of proteins and ligands and graphically rendered with PyMOL 1.7.6 [27]. PB potentials are given in units of $kT$ per unit charge ($k$, Boltzmann's constant and $T$, absolute temperature).

### Molecular Dynamics calculations

Alt a 1 systems explored with MD calculations were the following: (a) the butterfly-like dimers with and without intermolecular C30–C30 disulfide bridge, (b) the dimeric arrangement taken from the tetramer in complex with quercetin, and (c) the full tetrameric structure complexed with quercetin. Systems (b) and (c) were subjected to MD simulations at pH 5.5 and 6.5 using the CHARMM 3.1 force field [38] were performed with the multiprocessor Linux-POWER-MPI version of NAMD 2.10 [41] in CeSViMa supercomputer of Technical University of Madrid. All systems were immersed in periodic rectangular solvation boxes with a spacing distance of 15 Å around proteins and water molecules added according to the TIP3P model [42]. $Na^+$ and $Cl^-$ ions were added to counter the total charge of protein systems at the different pH values while providing 0.150 M salt concentration. The total number of atoms involved in these simulations were about 49,800, 50,500, and 74,000 for systems (a), (b), and (c), respectively. The particle mesh Ewald summation method [43] was used for long-range electrostatic and a 10 Å cutoff was set for short-range non-bonded interactions. For every system, the following set of calculations were done: (1) optimization along 5000 conjugate gradient minimization steps, (2) equilibration of water for 100 ps at 2 fs time steps at 298 K and 1 atm with all atoms except those of water fixed, and (3) simulation runs during 100 ns keeping same time step (which involves 50 million steps for every simulation), and same T and P in the NPT ensemble. Langevin dynamics for T control and Nosé-Hoover Langevin piston method for P control were used. Output results were stored every 25,000 steps rendering thus trajectories composed of 2000 frames which were processed and analyzed with VMD 1.9.2 [44].

## Results and Discussion

### Quaternary structure of Alt a 1 suggests a putative binding site in the tetrameric assembly

The crystal structure of Alt a 1 include residues 28 to 157 traced into electron density [14]. Searches for related topologies using PTGL provided no match for Alt a 1 architecture. This unique topology features an 11-stranded β-barrel fold with one 3-residue $3_{10}$ helix (Fig. 1). Four cysteines forming intramolecular C74–C89 and C128–C140 disulfide bridges are conserved among all sequences of Alt a 1 homologs whereas a fifth N-terminal cysteine C30 is only conserved among the closest homologs [14]. Three residues (Y46, D114, and V139) have 0.50 occupancy in electron density map thus indicating two alternative conformations. While both conformations are similar in V139, they differ noticeably by torsion at Cβ position in D114 and particularly in Y46 (Fig. 1). As shown below, one of the two side chain orientations of this tyrosine is involved in ligand-binding.

PISA predicts two quaternary structure aggregates: a tetramer with total buried area 11290 $Å^2$ and solvation free energy change upon assembly of $-186$ kcal $mol^{-1}$ (Fig. 2a) and a dimer in a butterfly-like shape with total buried area 4870 $Å^2$ and solvation free energy change of $-106$ kcal $mol^{-1}$ (Fig. 2b). Some small compounds originated from the crystallization solution are present in the crystal structure. Although one would consider it unlikely that their spatial locations arising from symmetry operations that set oligomerization states could bear physiological significance, the location of two molecules of one of these compounds (4-hydroxy-2,5,6-triaminopyrimidine, Fig. 2c) is illuminating. They are located in the interface between two pairs of subunits in the middle of a barrel-like substructure made of β-strands from two different chains in tetramer (Fig. 2d). Moreover, this location displays a π-stacking geometry with two neighbor side chain rings of Y46 residues from different chains just in only one of their two possible conformations (B conformation in the crystal structure file). Taken together, these features led us to tentatively assume that this inter-monomer barrel could be a putative binding site of Alt a 1 in its tetrameric state.

### An intermolecular disulfide bridge is needed to stabilize dimeric Alt a 1

While its geometry clearly suggests that the butterfly-like dimer is linked by an intermolecular disulfide bond between C30 residues in the two chains (Fig. 2b) [14], evidence that Alt a 1 dimerization is not mediated by that link has been also reported [15]. As said above, it should be further considered that C30 is only conserved among the closest homologs of Alt a 1 [14]. To investigate the role played by C30 on the dimer stability in solution, we performed 100-ns MD simulations on the dimeric structure with and without that intermolecular disulfide bridge. Exploratory MD calculations during 20-ns simulation times had previously shown no other difference than larger RMSD values of backbone atoms that increased with time in the dimer without disulfide link [19]. However, by extending simulation time to 100 ns, we found here a

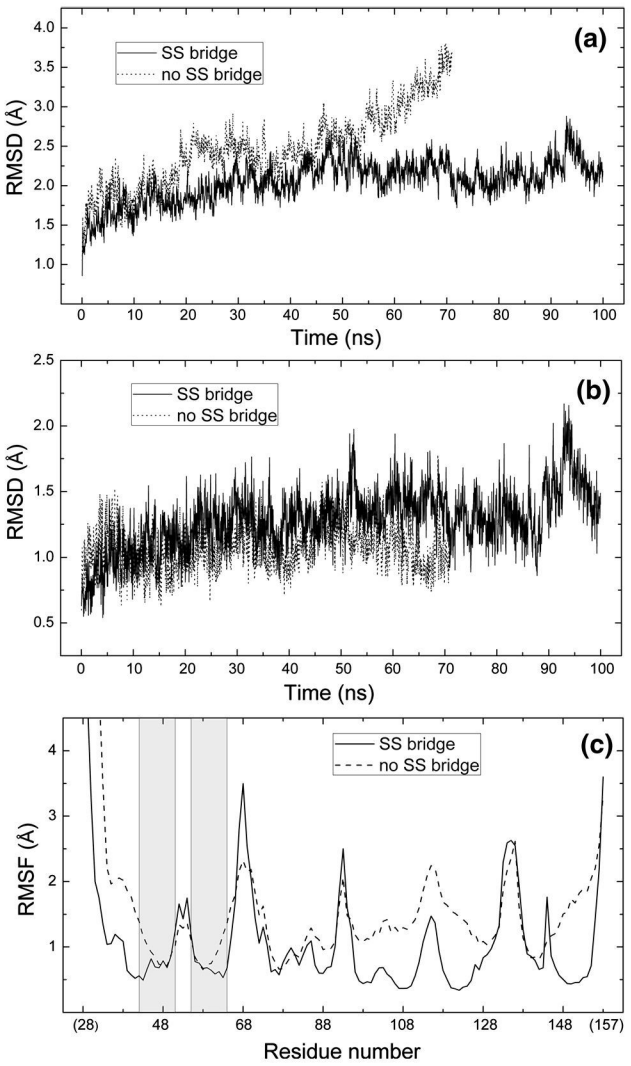


**Fig. 3** Results from 100-ns MD simulations of the butterfly-like dimeric form of Alt a 1 with and without the intermolecular disulfide bridge between C30 residues in the two chains. RMSD of backbone atoms in **a** the whole dimer and **b** residues in the two main IgE epitope regions [13]. **c** RMSF of all residues (28–157) present in the crystal structure of Alt a 1 [14]. Shaded segments 41–50 and 54–63 correspond to the two epitope regions

significant increase in backbone RMSD values at ~50 ns in the dimer without disulfide link that finally breaks down at t = 71 ns (Fig. 3a). Interestingly, the structural regions corresponding to the two main IgE epitopes, segments 41–50 and 54–63 [13] that span strands β1 and β2 together with loop β1β2 (Figs. 1b, 2b), show much smaller motion (Fig. 3b: compare scale with Fig. 3a). Furthermore, the intermolecular disulfide bond has no apparent effect on the mobility of epitope regions even at the time immediately before breaking (Fig. 3b). When time fluctuation (RMSF) of residues are compared, the absence of the intermolecular link reflects into overall greater fluctuations but RMSF values of epitope residues are consistently low in the presence and in the absence of the disulfide bridge (Fig. 3c). One could speculate that local rigidity of epitope structural regions should be beneficial for cross-linking IgE interaction.

## Docking calculations predict a high-affinity tetrameric Alt a 1-quercetin complex

In the course of our preliminary work to identify the natural ligand of Alt a 1, our experimental results (to be published) show that at pH 6.5 Alt a 1 tetramerizes in the presence of quercetin while at pH 5.0–5.5 the assembly apparently breaks down. pH 6.5 is the value found in culture supernatant of bronchial epithelium [45] and hence it represents the expected acidity which Alt a 1 would meet with when it is secreted by *Alternaria* spores in bronchial epithelium. pH 5.0–5.5 is the value in the apoplast of ripe fruit [46] in which Alt a 1 would enter when infecting plant cells. It is worth noting that similar pH-dependence of both aggregation states and binding abilities are known for other proteins. It is the case of transthyretin, an amyloidogenic protein for which a crystal structure corresponding to the tetrameric form of a complex just with quercetin has been recently reported [47]. This tetramer structure shows two binding sites at inter-subunit interfaces and disrupts at pH 4.6 [48].

Based on the mentioned quercetin-binding evidence, 3D structures of Alt a 1-quercetin complexes were explored in silico by means of docking calculations. We firstly selected as search space a large 80 Å edge cube centered at the center of the tetramer enclosing the whole assembly structure and performed AutoDock Vina calculations to dock quercetin. The two best docking complex geometries (poses with lowest binding affinity free energies of −9.2 and −8.8 kcal/mol) proved to correspond to the two inter-chain sites in which two molecules of the crystallographic ligand are present in the PISA-predicted tetrameric structure (Fig. 2a). With this result, we then selected as search space a 20 Å edge cube centered at the middle point between aromatic rings of Y46 residues in neighbor chains (Fig. 2d) enclosing this site and performed new calculations to dock both quercetin and alternariol (Fig. 4a). *Alternaria* species produce over 70 secondary metabolites toxic to plants and some of them have been reported to be also toxic to humans and animals. Alternariol and alternariol methyl ether are the two most important mycotoxins produced by these fungi [49, 50].

Vina docking method allows for ligand flexibility [33]. While quercetin has freedom of rotation about the bond between 1-benzopyran-4-one and catechol rings, alternariol is a conjugate molecule (Fig. 4a) rigid in docking

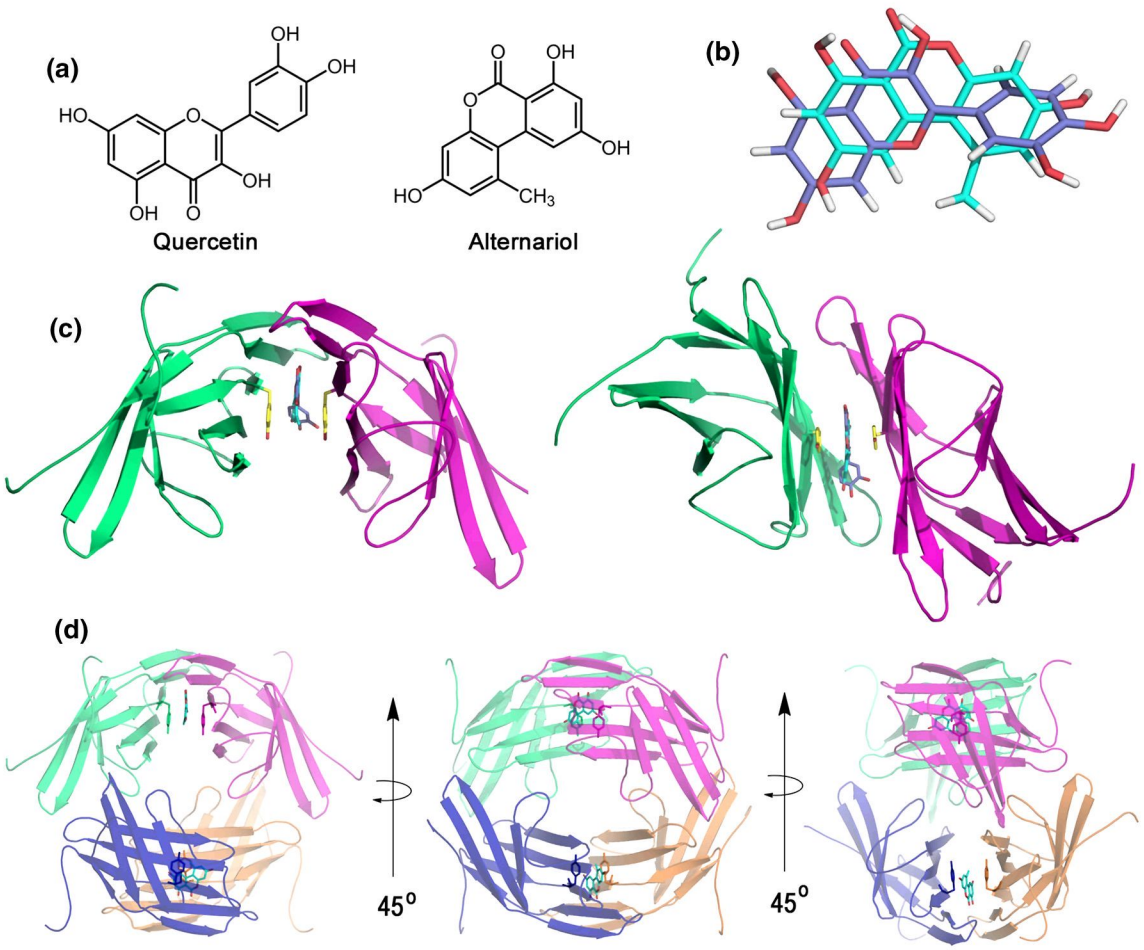


**Fig. 4** **a** Structural formulas of quercetin and alternariol used in docking calculations. **b** Geometries of quercetin (*deep blue sticks* for carbon bonds) and alternariol (*cyan sticks* for carbon bonds) from structural superposition of the corresponding complexes with tetrameric Alt a 1. **c** Upper (*left*) and side (*right*) views of the inter-chain binding site in the superimposed structures of tetrameric Alt a 1 complexes with quercetin and alternariol (same *colors* as in **b**). Side chains of Y46 residues in their conformation B are depicted as *yellow* sticks for carbon bonds in the two chains. **d** The two binding sites in tetrameric Alt a 1 are symmetry-related by a rotation by 90° about a *vertical* axis through the center of the tetramer. Three views rotated by 45° are shown

calculations although it is known to distort slightly from planarity upon intermolecular hydrogen bonding of OH groups [51]. Quercetin docked to tetrameric Alt a 1 has its catechol ring rotated a torsion angle of 67° with respect to benzopyran ring while docked alternariol remains planar (Fig. 4b). Most stable docked complexes predicted by Vina for this tetramer confirmed the binding site at the center of the inter-monomer barrel-like substructure identified above (Fig. 2). Y46 residues in conformation B from the two chains flank the site displaying a π-stacking arrangement with both ligands (Fig. 4c). Nine residues from each chain are within 4.5 Å neighborhood of quercetin which is also hold by three hydrogen bonds: two of them link both catechol hydroxyls to Nδ2 and Oδ1 atoms of Asn 61 in chain A and the third one links carbonyl oxygen of quercetin to Oε1 atom of Gln 141 in chain A (Fig. S1 in Supplementary Material). Superposition of quercetin and alternariol complexes showed nearly coincident locations for both ligands (Fig. 4b–d). Best docking modes of quercetin and alternariol showed affinity free energies of −9.3 and −9.5 kcal/mol, respectively. Taking these values as estimates of protein–ligand binding free energies would predict complex dissociation constants 0.13 and 0.093 μM, respectively. Separate dockings for the two possible sites in the tetramer gave exactly the same results. These two sites are symmetry-related by a rotation about an arbitrary axis joining their centers by 90° (Fig. 4d).

Docking of quercetin to monomeric Alt a 1 was also explored. To this end, we firstly selected as search space a large 50 Å edge cube centered at the center of the β-barrel enclosing the whole structure. The two best docking geometries (poses with lowest affinity free energies of

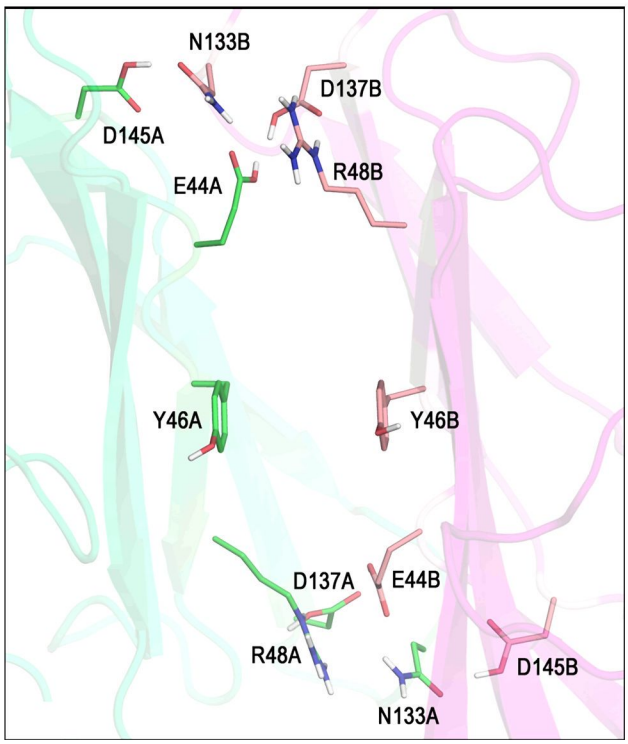


**Fig. 5** Interacting residues E44, R48, N133, D137, and D145 located at both ends of the barrel-like substructure in the interface between subunits in tetrameric Alt a 1. E44 and D137 are coupled residues with alternative protonation states. Y46 side chains are shown as a reference to locate ligand position in the putative binding site. *Letters* after residue labels denote A and B chains

−6.5 and −5.8 kcal/mol: Fig. S2 in Supplementary Material) corresponded approximately to the spatial locations of two molecules of the crystallographic ligand present in the monomer crystal structure (PDB id. 3V0R [14]). Whereas neither of these two poses lie inside the β-barrel (Fig. S2 in Supplementary Material), that of lower energy displays quercetin close to Y46 at a spatial location which corresponds to the barrel-like inter-chain site when monomers aggregate to form the tetramer (Fig. 2d and 4c). Additional docking calculations with the butterfly-like dimer and search spaces defined by a 50 × 50 × 80 Å box enclosing the whole structure found similar sites, neither of which are near the protein–protein interface in the dimer. Comparing docking affinity energies, structural features of binding sites, and protein–ligand interactions in the different oligomeric Alt a 1-quercetin complexes it seems apparent that the inter-chain barrel-like site in the tetrameric assembly (Fig. 4) is most favorable for binding.

## Predicted p*K*a shifts show a different pH-dependent pattern for different aggregation states of Alt a 1

p*K*a values of all residues with ionizable side chain groups were obtained with the empirical predictor Propka 3.1 [34, 35] for the three aggregation states of Alt a 1 (Table 1). The implementation in Propka 3.1 of new algorithms for modeling noncovalently coupled titrational events allow to predict the effect on p*K*a values of the spatial proximity of titratable groups that can influence the titration of each other. This improved version of the p*K*a predictor takes thus account on coupling effects between amino acid side chains and also incorporates effects between ligands and interacting residues [35].

Alt a 1 has a total of 38 titratable amino acids (arranged in ascending order of standard p*K*a's in water): 11 aspartates, 5 glutamates, 1 histidine, 1 cysteine not involved in intramolecular disulfide bonds, 8 tyrosines, 9 lysines, and 3 arginines (Table 1). At neutral pH (unprotonated histidine) this yields a total charge −4 for Alt a 1 protein. Among these 38 residues, 12 in tetramer, 8 in dimer, and 4 in monomer display p*K*a shifts from model values about 1.0 p*K*a unit or greater (they are highlighted in Table 1). Most of these residues are located at interfaces between subunits in the butterfly-like dimer and more prominently in the tetramer. One might therefore conjecture that changes of protonation states produced by pH variations could significantly affect oligomer stability. A remarkable exception to this location is the case of R48 and Y55 in the dimer that have their side chains highly exposed to the environment (Fig. S3 in Supplementary Material). If one considers that these two residues are within the 41-50 and 54-63 epitope regions proposed for Alt a 1 [13], it is tempting to speculate that R48 and Y55 could play a prominent role in the interaction with IgE. Other points regarding these p*K*a shifts ≥1.0 units are worth to note (Table 1): 2 out of the 3 residues with shifts ≥2.0 in tetramer (E44 and Y46) are at or near the putative binding site in the inter-subunit interface (Fig. S3b); Y46, which is here proposed to play a major role in protein–ligand interaction, has shifted p*K*a values only in tetramer; C30, which forms the intermolecular disulfide bond that stabilizes dimeric Alt a 1 as mentioned above, has shifted p*K*a values only in the dimer; R48, which is speculated to be involved in IgE interaction, has identical shifted p*K*a values in the three aggregation states.

As said, two ionizable groups at nearby spatial positions can influence titration of each other so that they titrate coupled. Propka 3.1 models such noncovalently coupled events by predicting p*K*a values in both of the two possible titrations thus yielding alternative protonation states [35]. In these cases, the method identifies which residues are interacting through backbone or/and side chain hydrogen bonding and Coulombic interaction. Sets of residues found to have alternative protonation states in aggregation states of Alt a 1 were: E44 and D137 only in tetramer, C30 only in dimer, and both Y38 and Y118 in the three states (Table 2). Since p*K*a's were computed without imposing

**Table 1** pKa values of residues with ionizable side chains in oligomerization states of Alt a 1

| Residue | Tetramer[a] | Dimer[a] | Monomer[a] |
|---|---|---|---|
| **D** | Model p*K*a = 3.80 | | |
| D37 | 3.26 | 3.20 | 3.16 |
| D71 | *4.85* | 3.83 | 3.83 |
| D79 | 3.93 | 3.90 | 3.90 |
| D83 | 3.16 | 3.85 | 3.16 |
| D96 | *4.78* | 4.54 | 4.29 |
| D100 | 4.06 | *4.86* | 4.06 |
| D102 | *2.43* | 3.05 | 2.43 |
| D114 | 3.77 | 3.58 | 3.64 |
| D115 | 4.38 | 3.96 | 3.94 |
| D137 | 3.67 | 2.57 | 2.57 |
| D145[b] | *5.99* (AB) *5.65* (CD) | 4.30 | 4.04 |
| **E** | Model p*K*a = 4.50 | | |
| E35 | 5.06 | 4.96 | 4.94 |
| E44[b] | *7.81* (AB) *8.37* (CD) | 4.83 | 4.81 |
| E51 | 4.52 | 4.50 | 4.50 |
| E82 | 4.39 | 4.41 | 4.39 |
| E91 | *5.75* | 4.73 | 4.73 |
| **H** | Model p*K*a = 6.50 | | |
| H84 | 6.64 | 6.09 | 6.64 |
| **C** | Model p*K*a = 9.00 | | |
| C30[c] | 9.05 | *8.08* | 9.05 |
| **Y** | Model p*K*a = 10.00 | | |
| Y38 | 10.05 | *11.50* | 9.80 |
| Y46[b] | *11.81* (AB) *12.31* (CD) | 10.38 | 10.38 |
| Y54 | 10.40 | 10.40 | 10.40 |
| Y55 | *12.12* | *12.12* | *11.93* |
| Y87 | 10.00 | 10.27 | 9.95 |
| Y118 | *11.74* | 9.66 | *11.30* |
| Y127 | 9.85 | 10.13 | 10.13 |
| Y147 | *11.05* | 10.84 | 10.46 |
| **K** | Model p*K*a = 10.50 | | |
| K41 | 9.95 | 10.93 | 10.93 |
| K49 | 9.69 | 9.75 | 9.77 |
| K63 | 10.33 | 10.37 | 10.37 |
| K80 | 10.72 | 10.73 | 10.73 |
| K85 | 10.74 | 10.76 | 10.76 |
| K109 | 9.92 | *9.43* | 10.07 |
| K111 | 10.37 | 10.44 | 10.39 |
| K136 | 10.66 | 10.66 | 10.66 |
| K155 | 9.90 | *8.95* | 9.84 |
| **R** | Model p*K*a = 12.50 | | |
| R48 | *13.45* | *13.48* | *13.48* |
| R103 | *14.28* | *14.36* | *14.28* |
| R129 | 12.37 | 12.40 | 12.40 |

[a] Italicized values represent p*K*a shifts about 1 p*K*a unit or greater

[b] Different values in tetramer for chains indicated in parentheses

[c] Cysteines 74, 89, 128, and 140 participate in intramolecular disulfide bridges

intermolecular disulfide bridge in the dimer, the alternative p*K*a values of C30 in the two chains just reflect the close proximity of SH groups which form the disulfide link. Coupled alternative p*K*a's arising from vicinity of Y38 and Y118 in monomer (Fig. S4 in Supplementary Material) also reveal their mutual interaction. Alternative p*K*a's for

**Table 2** Residues with alternative p*K*a values in oligomers of Alt a 1

| Residue | Tetramer[a] | Dimer[a] | Monomer |
|---|---|---|---|
| D137 | 3.67 (ABCD) | | |
| | 5.78 (ABCD) | | |
| E44 | 7.81 (AB) 8.37 (CD) | | |
| | 5.69 (AB) 6.26 (CD) | | |
| C30 | | 8.08 (A) 10.16 (B) | |
| | | 10.16 (A) 8.08 (B) | |
| Y38 | 9.97 (CD) | 11.50 (AB) | 9.80 |
| | 11.46 (CD) | 10.01 (AB) | 11.21 |
| Y118 | 11.74 (CD) | 9.66 (AB) | 11.30 |
| | 10.25 (CD) | 11.15 (AB) | 9.88 |

Alternative p*K*a values are given in separate lines for each residue

[a] Chains indicated in parentheses

E44 and D137 in tetramer arise from their mutual interaction and from interactions (Coulombic and hydrogen bonding as well: data not shown) with R48, N133, and D137. Interestingly, all these residues are located at both ends of the barrel-like inter-chain substructure in the tetramer which is here proposed as the putative binding site of Alt a 1 (Fig. 5). As for these results, one might expect that changes in the protonation states of acidic E44 and D137 (occurring at pH 5.5–6.5) associated to their interaction with basic R48 (Table 2; Fig. 5) would affect protein–protein interfaces and hence the own tetramer stability.

A major feature of all these p*K*a predictions is that tetrameric Alt a 1 displays varying protonation states just between pH 5.0 and 6.5, interval of interest to further study the molecular processes that eventually lead to *Alternaria*-induced allergy or respiratory disorders. As a consequence of those different protonation states, the total charge of tetrameric Alt a 1 changes considerably between pH 5.0 and 6.5 whereas that of the dimer changes only 2 units and the total charge of monomeric Alt a 1 remains constant in that pH interval (Table 3).

## Poisson-Boltzmann electrostatic potentials of tetrameric Alt a 1 show pH-dependent major variations

Considering the great variations of total charge with pH found in tetrameric Alt a 1 and aimed to explore charge distribution over the protein surface, we computed Poisson-Boltzmann (PB) electrostatic potentials of this aggregate with ionizable side chains at protonation states corresponding to pH 5.5, 6.0, 6.5, and 7.0. The electrostatic nature of the surface shows marked differences (Fig. 6a, b). The outer surface exhibits large patchs of negative potential that span particularly over the middle hole in the structure at pH 7.0. In contrast, these areas show a much more positive potential at pH 5.5 (Fig. 6a). The inner surface region in the barrel-like inter-chain substructure also exhibits noticeable differences at the putative ligand-binding site. This site is dominated by a strongly negative potential that spans over the whole interface at pH 7.0 whereas it is lined with neutral/positive potential regions at pH 5.5 (Fig. 6b). The 0.0 PB electrostatic potential isosurface divides space around a molecule in negative and positive spatial domains (Fig. 6c). In the case of tetrameric Alt a 1 and despite its intricate shape, this isosurface shows a qualitatively distinct feature at pH 7.0 and 5.5. Whereas at neutral pH the middle hole is largely accessible because the 0.0 isosurface changes locally very close to the structure matching the protein topography, at pH 5.5 the isosurface extends outwards from the structure (Fig. 6c).

Given the large p*K*a differences noticed above, we performed new docking calculations of quercetin and alternariol to tetrameric Alt a 1 now with the protonation states corresponding to pH 5.5, 6.0, 6.5, and 7.0. Except for the conformation of some hydroxyl hydrogens, geometries of docked quercetin at all those pH values are rather similar (Fig. S5 in Supplementary Material; the same was found for docked alternariol: data not shown). The PB electrostatic potential computed for quercetin molecule mapped onto the molecular surface shows slightly positive dominant character when (Fig. 6d), although it has a smaller range of values than protein (see scale bar in Fig. 6). Thus, in complexes in which the binding site is more negative, i.e. at higher pH's (Fig. 7), one might expect a stronger protein–ligand affinity than at lower pH's. This is in agreement with the aforementioned result that Alt a 1 tetramerizes in the presence of quercetin at pH 6.5 but not at pH 5.5. Finally, it must be noted that the interfaces between subunits in the tetramer leave enough room for access of ligands (Fig. 7).

## MD simulations show a pH-dependent pattern for stability of tetrameric Alt a 1-quercetin complex

The stability of tetrameric Alt a 1-quercetin complexes in solution at different pH values was addressed by means of 100-ns MD simulations. A first set of MD calculations were performed for a model dimer composed of two neighbor chains forming the barrel-like binding site (Fig. 4c) taken from tetramer complexes prepared with docking calculations at different pH́s as explained above. A second set of MD calculations were performed for the full tetrameric assembly of these complexes with quercetin. Given the considerable computational effort involved in tetramer forms (over 74,000 atoms and 50 million simulation steps), they were restricted to the complexes at the two most representative pH values mentioned above: 5.5 and 6.5. In order to compare the pH-dependence pattern

**Table 3** Total charge of oligomerization states of Alt a 1 at different pH's

| pH | Tetramer | | Dimer | Monomer |
|---|---|---|---|---|
| | Normal p*K*a state | Alternative p*K*a state | | |
| 7.0 | −12 | −16 | −8 | −4 |
| 6.5 | −8 | −12 | −8 | −3 |
| 6.0 | −6 | −8 | −6 | −3 |
| 5.5 | 0 | +4 | −6 | −3 |
| 5.0 | +4 | +8 | −6 | −3 |
| 4.5 | +16 | +20 | +6 | +1 |

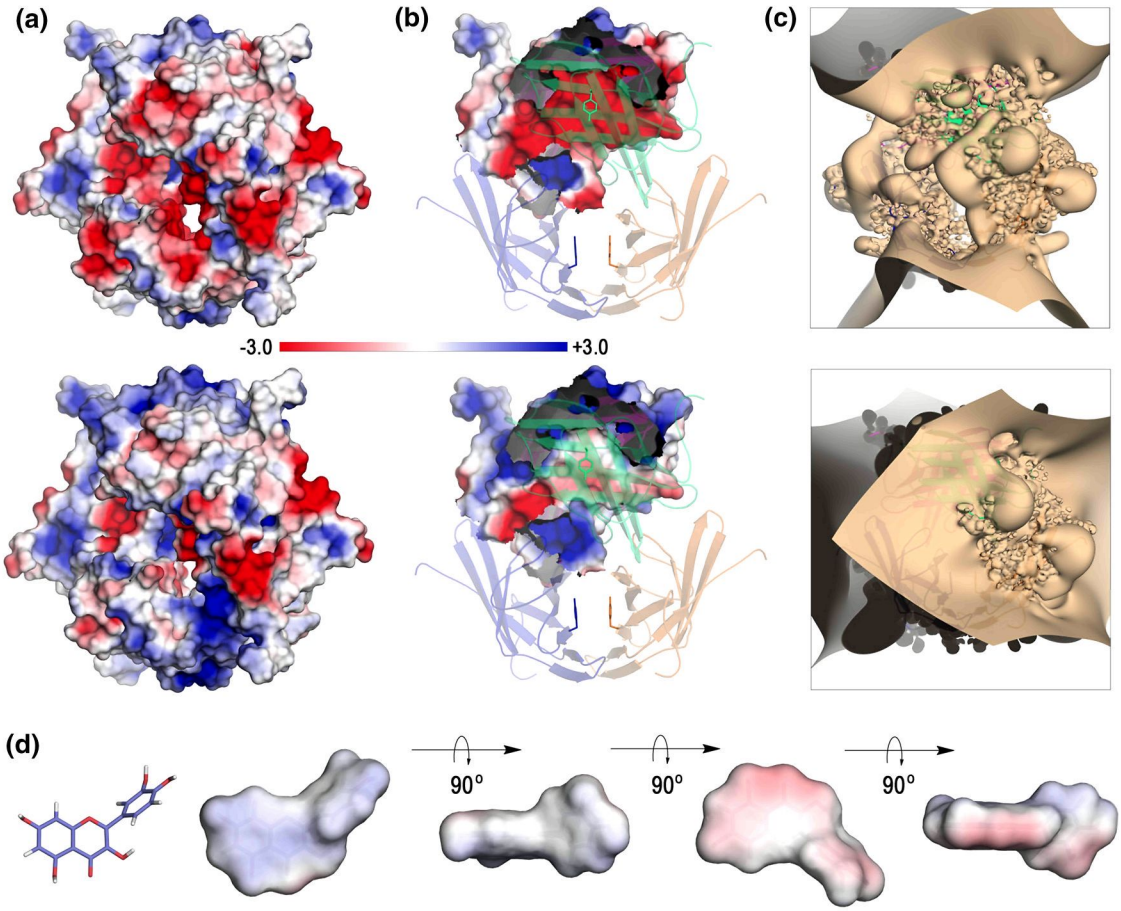


**Fig. 6** **a** PB electrostatic potential mapped onto the outer surface of tetrameric Alt a 1 with ionizable side chains at protonation states corresponding to pH 7.0 (*top*) and 5.5 (*bottom*). The structure is seen at the same orientation as the last view in Fig. 4d. **b** PB potential mapped onto the inner surface of one of the two inter-subunit interfaces forming the putative binding site. Same orientation and pH values as in **a**. Side chains of Y46 (sticks in same *colors* as *chain ribbons*) are shown as a reference to locate ligand position. **c** 0.0 Isosurfaces of PB electrostatic potential at same orientation and pH values as in **a**. **d** Geometry of quercetin and PB potential mapped onto its molecular surface at four views rotated by 90° about a horizontal axis. Same scale range of PB potential used in **a** and **b**

provided by MD simulations for dimer and tetramer forms, the results analyzed here refer to the dimeric interface with quercetin bound in the putative binding site. In what follows, it must be taken into account that all the RMSD values analyzed (Fig. 8), including those of the ligand, were computed along the trajectories upon aligning whole protein backbones, not the ligand.

In the dimer form, RMSD's of protein backbone atoms at both pH's display an overall similar pattern just until the complex at pH 5.5 breaks down sharply at 77.2 ns

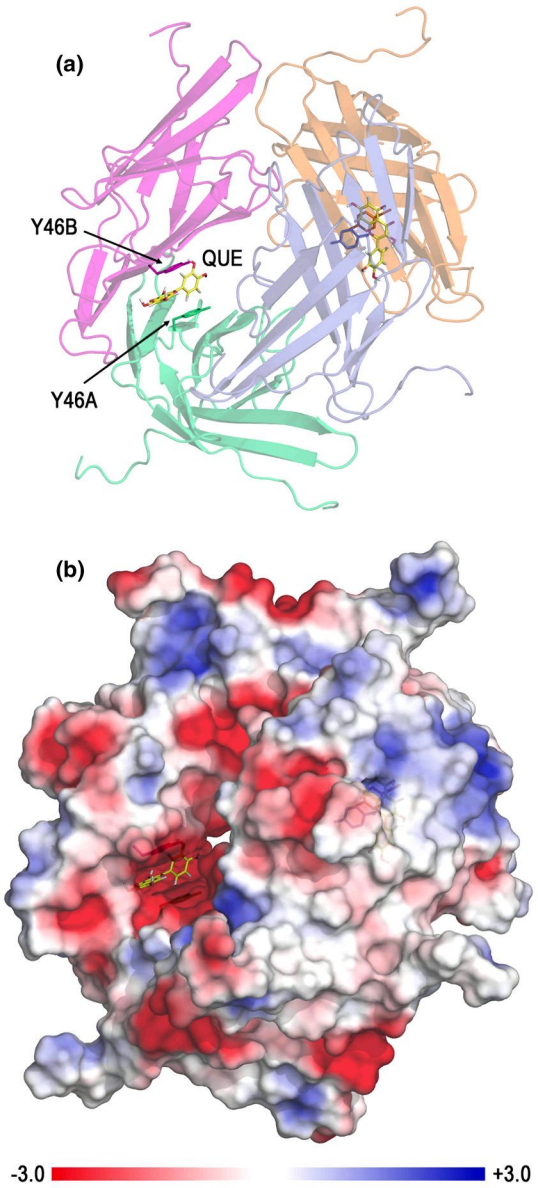


**Fig. 7** **a** Ribbon diagram of tetrameric Alt a 1-quercetin (QUE: *yellow sticks* for carbons) complex with ionizable side chain groups at protonation states corresponding to pH 7.0. Side chains of Y46 (*sticks* in same *colors* as chain ribbons) in the binding site are also shown. **b** PB electrostatic potential mapped onto the surface of tetrameric Alt a 1 at same pH and orientation as in **a** in a perspective to view the location of quercetin in the binding site

(Fig. 8a). The ligand exhibits a markedly different behavior. At pH 6.5, RMSD's of non-hydrogen quercetin atoms show values ~5 Å during the first 60 ns that decrease down to ~3 Å during the next 30 ns ending up again at ~5 Å (Fig. 8b). At pH 5.5, quercetin RMSD values are initially very low (<2 Å) and increase then at 35 ns showing greater variations until this dimer disrupts at 77.2 ns (Fig. 8b).

In the tetramer form, RMSD's of protein backbone atoms at pH 6.5 increase during the first half of the simulation and then stabilize at values ~4 A (Fig. 8c). Note that despite these RMSD's refer now to the whole tetrameric system, their magnitude is similar to those of the dimeric system. At pH 5.5, these RMSD's remain low during nearly the first half of the simulation but they increase rapidly around 50 ns and tetramer complex breaks down at 50.6 ns (Fig. 8c and Fig. S6 in Supplementary Material). The behavior of quercetin predicted by MD simulations for this tetramer form is again rather different. At pH 6.5, RMSD's of non-hydrogen quercetin atoms increase considerably during the first half of the simulation and then decrease stabilizing at about 5 Å during the second half of the simulation (Fig. 8d). At pH 5.5, quercetin RMSD values are again initially low but they show intense oscillations at 45 ns just before breaking at 50.6 ns (Fig. 8d). Marked oscillations in RMSD plots for quercetin (particularly in tetramer complex) might be viewed as a consequence of the motion of large protein systems in which, besides, the long N-terminal tails (Fig. 4c, d) have a great mobility in solution.

It must be stressed that MD simulations for both dimer and tetramer forms agree in predicting system breakdown at pH 5.5 and system stability at pH 6.5. Given the differences in mobility, structure complexity, and aqueous environments involved in dimer and tetramer systems on one side, and the fact that initial structures for the dimeric interface analyzed are the same in both cases (p*K*a predictions do not change protein structure), this MD result should be associated with different protonation states underlying both pH's. The shorter simulation time at which breakdown occurs in the tetramer with respect to the dimer at pH 5.5 hints at a slightly greater lability of the tetrameric complex. If one recalls that 5.5 is the expected pH that Alt a 1 would meet in the apoplast when infecting plant cells and that 6.5 is a pH typical of bronchial epithelium where the protein would be secreted by *Alternaria* spores, these MD results suggest that tetrameric Alt a 1-quercetin complex should be dynamically unstable in the location of Alt a 1 in infected plants and stable in infected humans. In any event, it is obvious that the complex breakdown process predicted by these MD calculations must be investigated deeper, which is beyond the scope of this computational report on Alt a 1 protein.

Finally, it is noted that protein–ligand nonbonded energies computed from these MD trajectories also reveal the pH-dependence discussed. Plots of electrostatic and van der Waals protein–ligand interaction energies in both dimer and tetramer forms show significant changes just during 5–10 ns before complex breakdown at pH 5.5 whereas they behave steadily at pH 6.5 during that time span (Fig. S7 in Supplementary Material). In the dimer form, both energies are similar during most of the time at both pHs except just in the last 5 ns at pH 5.5 in which the electrostatic term

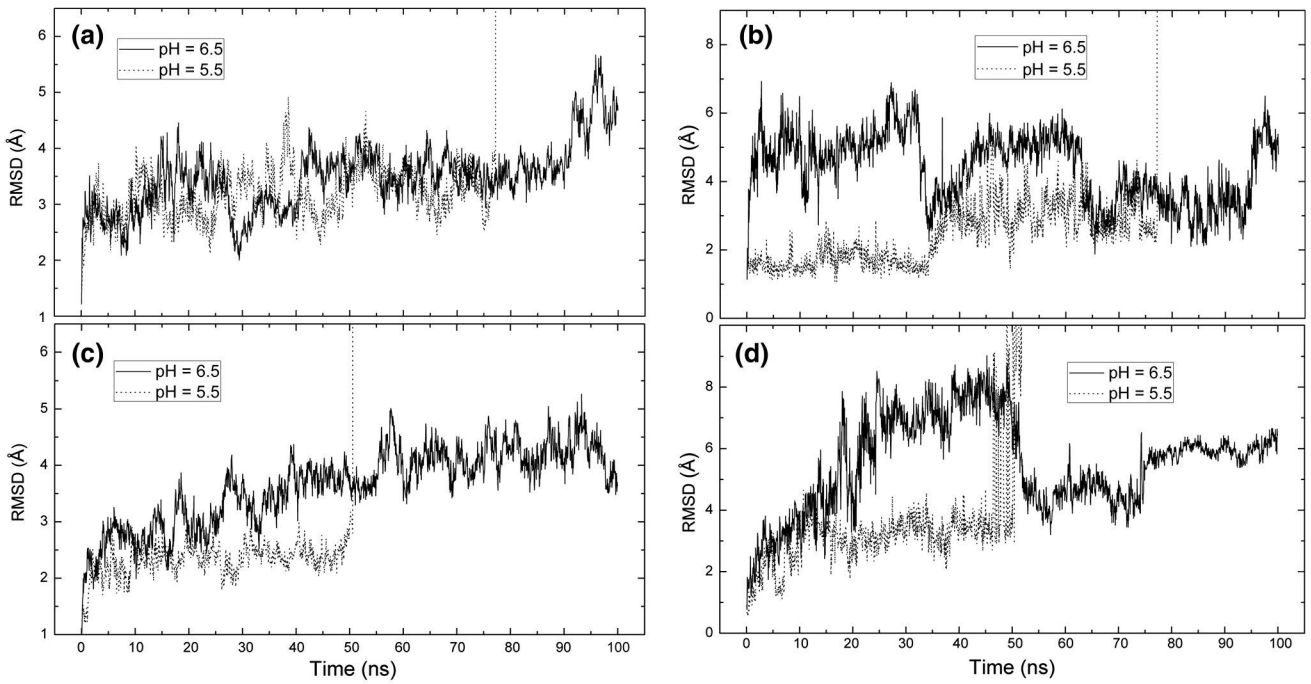


**Fig. 8** RMSD results for the dimeric interface forming the barrel-like binding site in the tetrameric Alt a 1-quercetin complex at pH 5.5 and 6.5. RMSD of **a** protein backbone atoms and **b** non-hydrogen atoms in quercetin from 100-ns MD simulation in the dimer form (Fig. 4c). Dimer complex at pH 5.5 breaks down at 77.2 ns. RMSD of **c** protein backbone atoms and **d** non-hydrogen atoms in quercetin from 100-ns MD simulation in the complete tetramer form (Fig. 4d). Tetramer complex at pH 5.5 breaks down at 50.6 ns

increases sharply even becoming repulsive (Fig. S7a) whereas the vdW term shows no noticeable changes (Fig. S7b). In the tetramer form, the interaction energies differ during most of the time although they show most marked changes during the last 10 ns before breakdown at pH 5.5, time span in which both electrostatic (Fig. S7c) and vdW (Fig. S7d) energies become much less attractive at this pH than at 6.5. As far as these non-bonded protein–ligand energies computed over MD simulations are concerned, these results suggest again that Alt a 1-quercetin complex should be favored at pH 6.5 but not at 5.5. The variation of protein–ligand electrostatic energies along MD simulations is thus in agreement with the discussion on PB electrostatic potential features presented above.

## Conclusions

Alt a 1, a highly allergenic protein from *Alternaria* sp. fungi is particularly interesting because of its structural peculiarities [14]. The monomer shows a unique β-barrel fold that is at odds with other proteins featuring this substructure as the barrel seems too narrow to harbor any ligand. Alt a 1 forms a highly symmetric butterfly-like homodimer with a geometry which favors an intermolecular disulfide bond but evidence against this link has been also reported [15]. Studies of IgE-binding with sera from *Alternaria*-sensitized patients allowed to identify two major epitope regions [13] that display a structural organization appropriate for cross-linking in IgE-interaction. Alt a 1 is predicted to form also stable tetrameric assemblies but no other information regarding this oligomer is available. The biological function of Alt a 1 is still unknown yet its localization in cell wall of *Alternaria* spores [17] that mediate allergic reactions and its possible role in spore germination [18] should be consistent with a function of transporter of small ligands but, as said, the β-barrel is apparently unable to bear ligands. Further, our experimental results reveal that the tetrameric assembly of Alt a 1 binds quercetin but both the own aggregation state and ligand binding abilities are pH-dependent, a behavior which, incidentally, is also known for other quercetin bearing proteins [47, 48]. It seems thus that the different oligomers could play different roles, a feature that we think should be particularly relevant to study physiological interactions of Alt a 1 involved in the onset of allergic reactions.

Our computational study on the structural features of Alt a 1 conducted within a research programme aimed at elucidating physiological interactions involved in *Alternaria* allergy led us to propose the following tentative picture. Alt a 1 tetrameric assembly is favored in the presence of an as yet unknown ligand which is well represented by the flavonoid quercetin. The corresponding tetramer-ligand

complex displays two symmetric barrel-like substructures composed of β-strands from different chains that we suggest is the binding site of Alt a 1. The ligand locates at the interface between subunits in the middle of the barrel flanked by nearby aromatic rings of two tyrosines (Y46) from different chains at a proper geometry for π-staking interaction. This geometry corresponds precisely to one of the two alternative conformations of Y46 derived from electron density in the reported high-resolution crystal structure of Alt a 1 [14]. Different protonation states of ionizable side chain groups arising from different pH's modify protein–ligand affinity so that the quercetin complex is electrostatically favored at pH $\geq$ 6. Since the pH which Alt a 1 would meet in bronchial epithelium is 6.5, the tetrameric form should be the favored state of the protein there. In contrast, MD simulations show that this complex disrupts at pH 5.5 so that one might expect that the monomer should then be the favored state. However, if one takes into consideration the suggestion that high local concentrations of protein favor dimerization [15], that the dominant state of Alt a 1 would ultimately be either monomeric or dimeric should depend on local concentration. In this regard, it must be recalled that the symmetric dimer in the butterfly-like shape (which indeed presents proper orientation of epitope regions [13] for IgE cross-linking) could be the favored state of Alt a 1 protein upon local high concentration.

Additional in silico work is obviously still needed to elucidate details concerning oligomerization and ligand-binding features of Alt a 1. However, we believe that the results presented here are of interest for further in vitro and in vivo work aimed at elucidating not only the biological function of this protein but also its physiological interactions related with allergy and other respiratory diseases in humans associated to *Alternaria* genus. Research along these lines is underway in our laboratory and will be the subject of forthcoming reports.

**Acknowledgments** All Molecular Dynamics calculations were carried out on the Magerit supercomputer of Universidad Politécnica de Madrid. The authors acknowledge the computer resources and technical assistance provided by the Centro de Supercomputación y Visualización de Madrid (CeSViMa). This work was supported by the Spanish Ministerio de Ciencia e Innovación MINECO (Grant BIO2013-41403-R) and Instituto de Salud Carlos III, Spain, RETICS 2007 (RD12/0013/14). CGC was supported by the FPI programme from Spanish Government (MICINN/MINECO, Grant BES-2010-034628).

## References

1. Delfino RJ, Zeiger RS, Seltzer JM, Street DH, Matteucci RM, Anderson PR et al (1997) The effect of outdoor fungal spore concentrations on daily asthma severity. Environ Health Perspect 105:622–635
2. Bush RK, Portnoy JM (2001) The role and abatement of fungal allergens in allergic diseases. J Allergy Clin Immunol 107:S430–S440
3. Anderson M, Downs S, Mitakatis T, Leuppi J, Marks G (2003) Natural exposure to *Alternaria* spores induces allergic rhinitis symptoms in sensitized children. Pediatr Allergy Immunol 14:100–105
4. Bush RK, Prochnau JJ (2004) *Alternaria*-induced asthma. J Allergy Clin Immunol 113:227–234
5. Knutsen AP, Bush RK, Demain JG, Denning DW, Dixit A, Fairs A et al (2012) Fungi and allergic lower respiratory tract diseases. J Allergy Clin Immunol 129:280–289
6. Salo PM, Arbes SJ, Sever M, Jaramillo R, Cohn RD, London SJ, Zeldin DC (2006) Exposure to *Alternaria alternata* in US homes is associated with asthma symptoms. J Allergy Clin Immunol 118:892–898
7. Feo Brito F, Alonso AM, Carnes J, Martin-Martin R, Fernandez-Caldas E, Galindo PA et al (2012) Correlation between Alt a 1 levels and clinical symptoms in *Alternaria alternata*-monosensitized patients. J Invest Allergol Clin Immunol 22:154–159
8. Deards MJ, Montague AE (1991) Purification and characterization of a major allergen of *Alternaria alternata*. Mol Immunol 28:409–415
9. De Vouge MW, Thaker AJ, Curran IH, Zhang L, Muradia G, Rode H et al (1996) Isolation and expression of a cDNA clone encoding an *Alternaria alternata* Alt a 1 subunit. Int Arch Allergy Immunol 111:385–395
10. Vailes LD, Perzanowski MS, Wheatley LM, Platt-Mills TA, Chapman MD (2001) IgE and IgG antibody responses to recombinant Alt a 1 as a marker of sensitization to *Alternaria* in asthma and atopic dermatitis. Clin Exp Allergy 31:1891–1895
11. Asturias JA, Ibarrola I, Ferrer A, Andreu C, Lopez-Pascual E, Quiralte J et al (2005) Diagnosis of *Alternaria alternata* sensitization with natural and recombinant Alt a 1 allergens. J Allergy Clin Immunol 115:1210–1217
12. Twaroch TE, Focke M, Fleischmann K, Balic N, Lupinek K, Blatt K et al (2012) Carrier-bound Alt a 1 peptides without allergenic activity for vaccination against *Alternaria alternata* allergy. Clin Exp Allergy 42:966–975
13. Kurup VP, Vijay HM, Kumar V, Castillo L, Elms N (2003) IgE binding synthetic peptides of Alt a 1, a major allergen of *Alternaria alternata*. Peptides 24:179–185
14. Chrusczc M, Chapman MD, Osinski T, Solberg R, Demas M, Porebski PJ et al (2012) *Alternaria alternata* allergen Alt a 1: a unique β-barrel protein dimer found exclusively in fungi. J Allergy Clin Immunol 130:241–247
15. Rouvinen J, Janis J, Laukhanen ML, Jylha S, Niemi M, Paivinen T et al (2010) Transient dimers of allergens. PLoS One 5:e9037/1-9
16. Wagner GE, Gutfreund S, Fauland K, Keller W, Valenta R, Zangger K (2014) Backbone resonance assignment of Alt a 1, a unique β-barrel protein and the major allergen of *Alternaria alternata*. Biomol NMR Assign 8:229–231
17. Twaroch TE, Arcalis E, Sterflinger K, Stoger E, Swoboda I, Valenta R (2012) Predominant localization of the major *Alternaria* allergen Alt a 1 in the cell wall of airborne spores. J Allergy Clin Immunol 129:1148–1149
18. Mitakakis TZ, Barnes C, Tovey ER (2011) Spore germination increases allergen release from *Alternaria*. J Allergy Clin Immunol 107:388–390
19. Garrido-Arandia M, Gómez-Casado C, Díaz-Perales A, Pacios LF (2014) Molecular dynamics of major allergens from *Alternaria*, birch pollen and peach. Mol Inf 33:682–694

20. Kabsch W, Sander C (1983) Dictionary of protein secondary structure: pattern recognition of hydrogen-bonded and geometrical features. Biopolymers 22:2577–2637
21. Touw WG, Baakman C, Black J, Te Beek TAH, Krieger E, Robbie P et al (2015) A series of PDB related databases for everyday needs. Nucleic Acids Res 43:D364–D368
22. Laskowski RA (2001) PDBsum: summaries and analyses of PDB structures. Nucleic Acids Res 29:221–222
23. Laskowski RA (2014) PDBsum additions. Nucleic Acids Res 37:D355–D359
24. May P, Barthel S, Koch I (2004) Protein topology graph library. Bioinformatics 20:3277–3279
25. Krissinel E, Henrick K (2007) Inference of macromolecular assemblies from crystalline state. J Mol Biol 372:774–797
26. Krissinel E (2010) Crystal contacts as nature's docking solutions. J Comput Chem 31:133–143
27. The PyMOL Molecular Graphics System, Version 1.7.6.4 Schrödinger, LLC
28. Pettersen EF, Goddard TD, Huang CC, Couch GS, Greenblatt DM, Meng EC, Ferrin TE (2004) UCSF Chimera: a visualization system for exploratory research and analysis. J Comput Chem 25:1605–1612
29. Siegel D, Troyanov S, Noack J, Emmerling F, Nehls I (2010) Alternariol. Acta Crystallogr Sect E 66:1366/1-7
30. Maier JA, Martinez C, Kasavajhala K, Wickstrom L, Hauser KE, Simmerling C (2015) ff14SB: improving the accuracy of protein side chain and backbone parameters from ff99SB. J Chem Theor Comput 11:3696–3713
31. Wang J, Wang W, Kollman PA, Case DA (2006) Automatic atom type and bond type perception in molecular mechanical calculations. J Mol Graph Model 25:247–260
32. Morris GM, Huey R, Lindstrom W, Sanner MF, Belew RK, Goodsell DS, Olson AJ (2009) Autodock4 and AutoDockTools4: automated docking with selective receptor flexibility. J Comput Chem 16:2785–2791
33. Trott O, Olson AJ (2009) AutoDock Vina: Improving the speed and accuracy of docking with a new scoring function, efficient optimization, and multithreading. J Comput Chem 31:455–461
34. Olsson MHM, Sondergaard CR, Rostkowski M, Jensen JH (2011) PROPKA3: Consistent treatment of internal and surface residues in empirical pKa predictions. J Chem Theor Comput 7:525–537
35. Sondergaard CR, Olsson MHM, Rostkowski M, Jensen JH (2011) Improved treatment of ligands and coupling effects in empirical calculation and rationalization of pKa values. J Chem Theor Comput 7:2284–2295
36. Dolinsky TJ, Nielsen JE, McCammon JA, Baker NA (2004) PDB2PQR: an automated pipeline for the setup, execution, and analysis of Poisson-Boltzmann electrostatics calculations. Nucl Acids Res 32:W665–W667
37. Dolinsky TJ, Czodrowski P, Li H, Nielsen JE, Jensen JH, Klebe G, Baker NA (2007) PDB2PQR: expanding and upgrading automated preparation of biomolecular structures for molecular simulations. Nucl Acids Res 35:W522–W525
38. MacKerell A, Bashford D, Bellott M, Dunbrack RL, Evanseck J, Field MJ et al (1998) All-atom empirical potential for molecular modeling and dynamics studies of proteins. J Phys Chem B 102:3586–3616
39. Baker NA, Sept D, Joseph S, Holst MJ, McCammon JA (2001) Electrostatics of nanosystems: application to microtubules and the ribosome. Proc Natl Acad Sci USA 98:10037–10041
40. Zoete V, Cuendet MA, Grosdidier A, Michielin O (2011) SwissParam, a fast force field generation tool for small organic molecules. J Comput Chem 32:2359–2368
41. Phillips JC, Braun R, Wang W, Gumbart J, Tajkhorshid E, Villa E et al (2005) Scalable molecular dynamics with NAMD. J Comput Chem 26:1781–1802
42. Jorgensen WL, Chandrasekhar J, Madura JD, Impey RW, Klein ML (1983) Comparison of simple potential functions for simulating liquid water. J Chem Phys 79:926–935
43. Darden T, York D, Pedersen L (1993) Particle mesh Ewald: an $N \log(N)$ method for Ewald sums in large systems. J Chem Phys 98:10089–10092
44. Humphrey W, Dalke A, Schulten K (1996) VMD—visual molecular dynamics. J Mol Graph 14:33–38
45. Fischer F, Wissicombe JH (2006) Mechanism of acid and base secretion by the airway epithelium. J Membr Biol 211:139–150
46. Almeida DPF, Huber DJ (1999) Apoplastic pH and inorganic ion levels in tomato fruit: a potential means for regulation of cell wall metabolism during ripening. Physiol Plant 105:506–512
47. Cianci M, Folli C, Zonta F, Florio P, Berni R, Zanotti G (2015) Structural evidence for asymmetric ligand binding to transthyretin. Acta Crystallogr Sect D 71:1582–1592
48. Pasquato N, Berni R, Folli C, Alfieri B, Cendron L, Zanotti G (2007) Acidic pH-induced conformational change in amyloidogenic mutant transthyretin. J Mol Biol 366:711–719
49. Barkai-Golan R (2008) *Alternaria* mycotoxins. In: Barkai-Golan R, Nachman P (eds) Mycotoxins in fruits and vegetables. Academic Press, San Diego, pp 185–203
50. European Food Safety Authority (2011) Scientific opinion on the risks for animal and public health related to the presence of *Alternaria* toxins in feed and food. EFSA J 9(2407):1–97
51. Garrido-Arandia M, Gómez-Casado C, Díaz-Perales A, Pacios LF (2014) Distortion from planarity in arenes produced by internal rotation of one single hydroxyl hydrogen: the case of alternariol. J Mol Graph Model 53:140–147